ELSEVIER

Colloids and Surfaces A: Physicochem. Eng. Aspects 238 (2004) 141–149

COLLOIDS AND SURFACES A

www.elsevier.com/locate/colsurfa

Polyethylene glycol penetration into clay films: real time experiments

Scott Baker [a], Roxana Begum [b], Peter Zalupski [b], Malaika Durham [b], Alanah Fitch [b,*]

[a] *Chicago State University, Chicago, IL, USA*
[b] *Loyola University Chicago, 6525 N. Sheridan Road, Chicago, IL 60626, USA*

Received 13 March 2002; accepted 29 December 2003

Abstract

The real time uptake of polyethylene glycol (PEG) into montmorillonite thin films is tracked by absorbance and clay-modified electrodes. The data indicate that there is a discontinuity in behavior observed between 600 and 1600 PEG related to the size of the PEG as compared to the interlayer dimensions within the clay film. Lower molecular weight PEG penetrate rapidly with little impact on co-diffusing probe molecules. At later times, the PEG slows penetration of the co-diffusing probe. Larger molecular weight PEG penetrate more slowly at all stages. In the initial stage the higher molecular weight species tend to disrupt the clay films, accelerating penetration of the co-diffusing probe molecule. Decrease in diffusion of the co-diffusing probe molecule is related to the formation of PEG domains within the interlayer region of the clay.

Keywords: Swy-1 montmorillonite; Thin clay films; PEG; Clay-modified electrodes

1. Introduction

Polyethylene glycol (PEG) is used as an additive to oil well drilling to prevent shales from expanding into the bore hole (Durand et al. [1]; Bailey et al. [2]). While the interaction of polyethylene glycol with clays under equilibrium conditions has been studied few studies mimic the in situ processes occurring during oil well drilling. During in situ processes PEG advances into the outmost layer of the shale forming a crust that prevents further motion of water into the shale (Kelly [3]; Reid and Dolan [4]). This study uses a variety of corroborative techniques to monitor the kinetics of the penetration of PEG into thin clay films. Two main methods are used: thin films supported over a micro-absorbance cell (Qui et al. [5]) and thin clay films supported on a Pt electrode (Fitch and Du [6]; Fitch and Subramanian [7]). Both methods provide complimentary information suggesting that the most effective PEG additives will be of intermediate chain length. Small chains are less effective in expulsion of water while longer chains are less effective in penetrating the clay film.

2. Materials and methods

Polyethylene glycols with molecular weights of 200, 600, 1500, 4600, and 10,000 amu (Aldrich) were used as received and stored under nitrogen to prevent degradation (Azaz and Segal [8]; Chang and Bock [9]). $Ru(NH_3)_6Cl_3$ (Alfa) was used as received. Standard Wyoming montmorillonite (SWy-1) (Source Clays Repository, University of Missouri, Columbia, MO) was purified in the following manner. Fifteen grams of clay were suspended in 450 ml of de-ionized water and stirred constantly for 48 h. The suspension was centrifuged at 3500 rpm to sediment particle sizes greater than 2 μm. This material was diluted to twice the volume with 2 M NaCl, solution stirred 36 h, then centrifuged for 45 min at 7000 rpm. The centrifugate was re-suspended in 2 M NaCl. The procedure was repeated twice. The centrifugate from the third suspension was re-suspended in

* Corresponding author. Tel.: +1-773-508-3119; fax: +1-773-508-3086.
E-mail address: afitch@luc.edu (A. Fitch).

0927-7757/$ – see front matter © 2004 Elsevier B.V. All rights reserved.
doi:10.1016/j.colsurfa.2003.12.034

de-ionized water, and dialyzed until no precipitate was found with 0.2 M $AgNO_3$. The sample was freeze-dried to remove all water.

Clay Film Preparation: A Pt mesh (100 LPI) was glued (Super Duper Super Glue) between two steel washers (i.d. diameter 4.0 mm). The lower washer was larger than the upper to provide a pressure seal to sensor block (see below). This washer assembly (WA) was cleaned before and after each clay film by tap water flush, a 4 h soak in a 2 M NaCl salt solution, and sonication in de-ionized water (twice) followed by sonication in 95% ethanol. Thickness of the dry clay films was estimated from the density of clay suspension added (17.5 g/l), the bulk density of the clay (1.77 g/cm^3) (Grim [10]), and the area inside of the washer above the platinum mesh. Thirty-three micrometers (dry thickness) films were made by covering a mesh area of 0.1257 cm^2 with three evaporations of 17.5 g/l clay suspension. The first 13 μl filled the holes between the mesh and air-dried for 1 h. The second aliquot (15.3 μl) was sedimented onto the first and dried overnight (12 h). The third aliquot (13 μl) was placed over the first two, 15 min allowed for wetting through the film, followed by spin-drying at 2000 rpm for one to 2 h. Air-drying was done at laboratory temperature and relative humidity. Temperatures varied from 72 to 79 °F and the percent relative humidity from 10 to 53% between winter and summer. The temperatures and relative humidities were monitored because adsorbed water can affect the rate of penetration of various solvents. All comparisons reported are matched for percent relative humidity.

The dry clay film coated WA was inserted diagonally into the solution filled acceptor cell (Fig. 1) of the sensor block and then allowed to settle to a horizontal position. The diagonal placement allowed air bubbles to be removed and proved to result in less mechanical failure of the film.

The sensor block was created from a grooved Teflon base mount. A fiber optic cable (Fiberguide Industries Inc.) was cut, polished with Al oxide abrasive with decreasing particle size (63–0.3 μm), aligned within the groove by monitoring the maximum light intensity recovered through the aligned cables and glued in place with optical adhesive (Norland Products Inc.). The final acceptor cell volume of 27 μl was obtained from the depth of the groove and the spacing of the cut fiber ends (2 mm). The donor cell, volume of 45 ml, was constructed by placing a PVC tube over the top of the WA with weights. The volume of the donor cell was relatively large to minimize the effect of concentration depletion so that the mathematical description of the system could be simplified (Kelly [3]).

The rest of the instrument was constructed from Oriel 77250 1/8 m Monochromator with an Oriel holographic grating Oriel #77296 set at 276 nm (for $Ru(NH_3)_6^{3+}$). The transmitted light was collected with LabVIEW and an interface board CIO-DAS08 (Computer Boards). The detection limit was based upon the stability of the Xe arc lamp and was found to be 1.28×10^{-4} for $Ru(NH_3)_6^{3+}$.

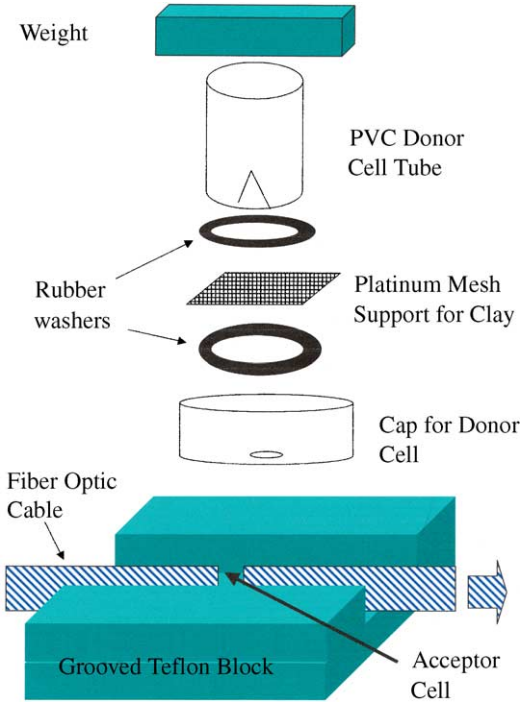

Fig. 1. Experimental setup for the micro-absorbance cell experiments. A fiber optic cable is embedded in a grooved Teflon block and a 2 mm section cut away to create a 27 μl volume acceptor cell. A 100 LPI Pt mesh is glued between two rubber washers. The donor cell is a PVC tube which is notched to provide access for removal and insertion of fluid. A weight holds all in place.

Electrochemical experiments were performed on clay films formed by spin coating either 10 μl of 17.5 g/l or 35 g/l clay suspensions over a Pt wire encased in glass (total area = 7.9×10^{-2} cm^2; Pt area = 7.85×10^{-3} cm^2). The dry thickness of the film was ~7.5 μm. Prior caliper measurements indicate that similar dry clay films range in thickness from 4 to 8 μm (Fitch et al. [11]). Prior scanning electron microscopy (SEM) measurements indicate that dry clay films thickness is ~6 μm (Joo and Fitch [12]). Films have been estimated to swell 40× in dilute salt leading ~315 μm (Kelly [3]). The wet film thickness was estimated to swell to the same extent taking account of the bulk density of the clay, the clay particle thickness and the dry clay film thickness (Subramanian and Fitch [13]). All experimental protocols and instrumentation for the clay-modified electrodes have been described elsewhere (Macha et al. [14]).

IR studies were performed by preparing clay suspensions with variable wt.% amounts of PEG, drying the suspension onto the washer assembly and monitoring the IR spectrum on a Mattson Genesis ATI Series FTIR.

Scanning electron microscopy of washer assemblies with clay films were performed on a Stereoscan 240 Scanning Electron Microscope (Cambridge Instruments/LEO Electron Microscopy, Thornwood, NY). In order to enhance the SEM imaging, the films were coated with a thin coat (300 Å or

0.03 μm) of Gold Palladium (60% gold/40% palladium) with a Hummer VI Sputtering system (Anateck Limited, Alexandria, VA). The original rubber washers used could not fit physically into the SEM sample holder (specimen stage), so smaller outside diameter metal washers were used to construct assemblies for the SEM analysis experiments. The inside diameter and thickness of these new washer assemblies were identical to the original rubber ones. The exact same 100 LPI platinum mesh was also used. Thin clay films were created using the same procedures and clay suspensions as described above.

3. Mesh supported films over micro-absorbance cells

$Ru(NH_3)_6^{3+}$ was selected as a probe molecule because of its relatively simple interaction with clay (non-adsorbing, diffuse double layer exchange), rapid transport through the film, its optical properties (Macha and Fitch [15]; Fitch et al. [16]), and its lack of interaction with PEG compounds. The lack of interaction was confirmed by monitoring the UV spectra of $Ru(NH_3)_6^{3+}$ in the presence and absence of the PEG. Since these experiments were conducted using a well-oriented SWy-1 clay film in low salt concentration (0.1 M NaCl) solutions the primary transport path for the probe molecule is through the interlayer regions of the clay.

Optimization of the experiment consisted of minimizing film thickness to the smallest film which could maintain integrity under the weight of the donor cell solution. SEM images indicate that the film is intact and self-sustaining in the 200 μm^2 holes formed by the Pt mesh (Fig. 2A). Stress lines along the clay connecting the clay film to the Pt wire are shown in Fig. 2B, while a perforation free space within the 200 μm^2 is shown in Fig. 2C. Self-sustaining films as thin as a calculated (based on bulk density and area) 11 μm could be formed with a 25% success rate.

Addition of PEG to the donor solution changed the topography of the film as shown by comparing Fig. 3A and B. The clay film exposed to $Ru(NH_3)_6^{3+}$ remained intact while a clay film exposed to both $Ru(NH_3)_6^{3+}$ and PEG 600 showed major disruptions. Such disruptions are expected to have an impact on the observed transport of the $Ru(NH_3)_6^{3+}$ probe molecule. An example of an experimental curve of concentration versus time for 5 mM $Ru(NH_3)_6^{3+}$ in 0.1 M NaCl and 5% PEG 600 is shown in Fig. 4 where concentration has been normalized by the maximum concentration observed, C/C_{max}, and the time has been normalized by the time at which the maximum concentration is observed, t/t_{max}. It is noted that the curve rises faster initially in the presence of PEG but with time the rate of penetration with PEG as compared to $Ru(NH_3)_6^{3+}$ only decreases.

Diffusion coefficients can be obtained from the transport data by either an analytical equation or a finite difference algorithm as described by Qiu (Qiu and Villemure [17]). The finite difference program is used in this report. The shape of a plot of C/C^*_{max} versus t/t_{max} can be fit by

$$\chi = \frac{j-1}{\sqrt{lD_{model}}} \quad (1)$$

where j is the number of volume elements in the finite diffusion program, l the iteration of time, and D_{model} is set to 0.45 for stability in the computation. The diffusion coefficient can be ascertained when the computational curve

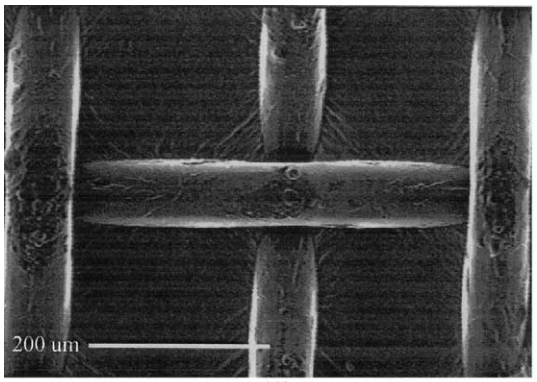

(A)

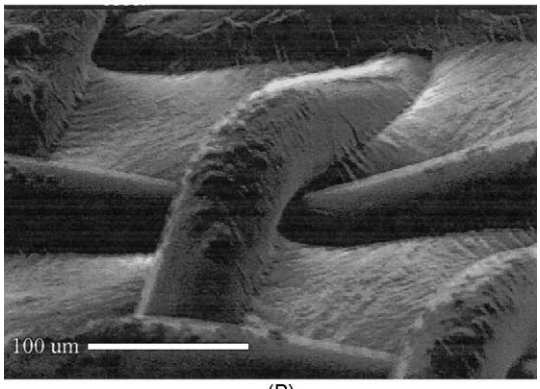

(B)

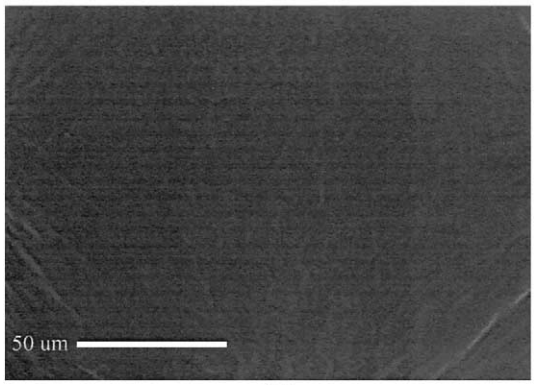

(C)

Fig. 2. (A) The 100 LPI Pt mesh covered with a calculated dry 11 μm thick SWy-1 clay film. The distance between Pt fibers is 200 μm, creating an unsupported clay film (200 $\mu m)^2$. (B) An angular exposure of the film illustrates the tension lines the occur between the clay on the Pt mesh and the clay in the unsupported region. (C) A closeup of the unsupported region shows a smooth film surface.

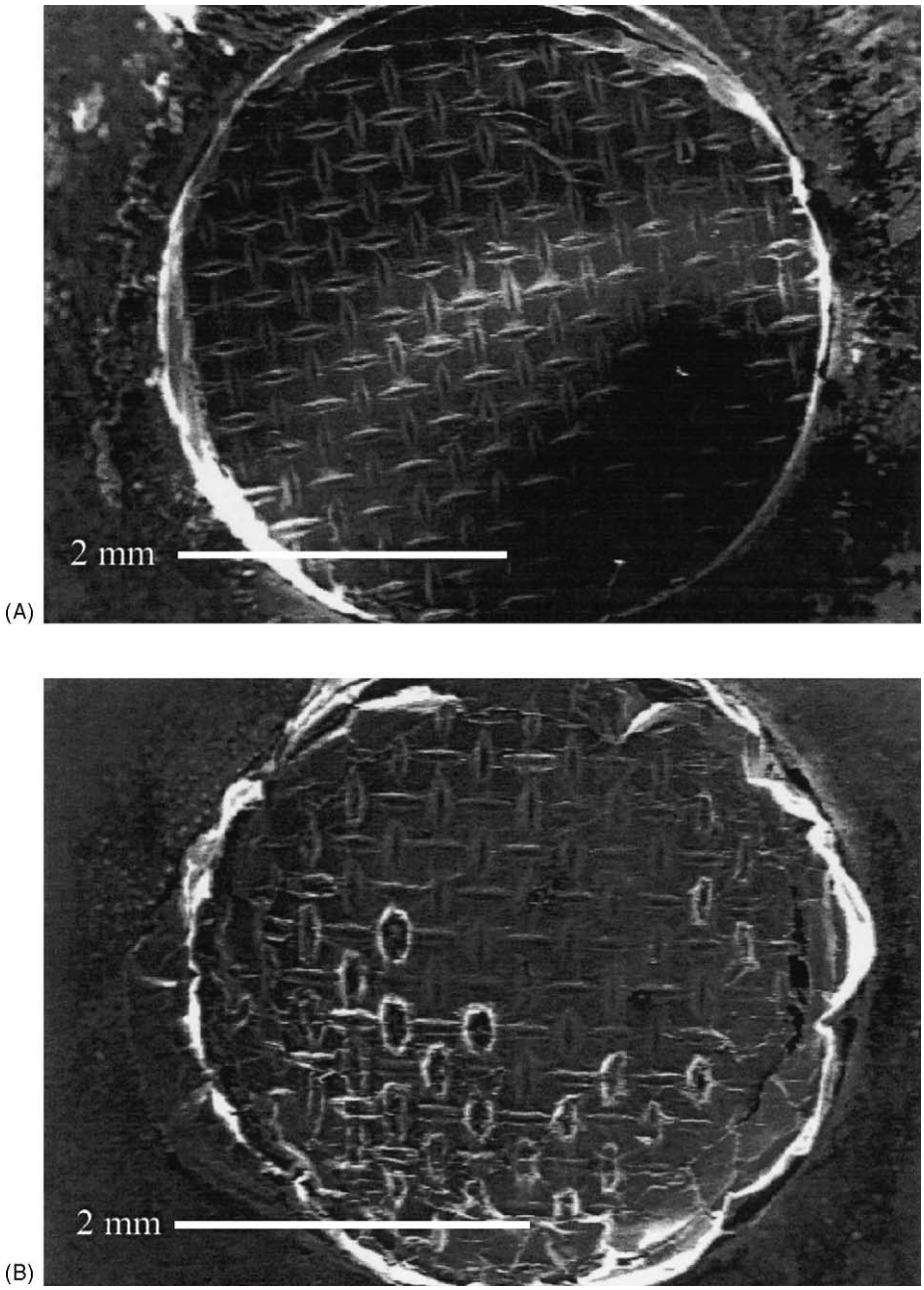

Fig. 3. (A) An SEM of a 33 μm thick (dry thickness) clay coated mesh after exposure to 5 mM $Ru(NH_3)_6^{3+}$ in 0.1 M NaCl solution. (B) An SEM of a 33 μm thick (dry thickness) clay coated mesh after exposure to 5 mM $Ru(NH_3)_6^{3+}$ in 0.1 M NaCl and 5% PEG600.

matches the experimental curve:

$$D = \frac{x\chi^2}{t} \quad (2)$$

where x is the wet film thickness and t is the experimental time of the experiment. The model is tested by determining the derived diffusion coefficient for $Ru(NH_3)_6^{3+}$ which was found to be 3.8×10^{-7} cm/s, consistent with other literature results (Fitch and Subramanian [7]). The finite difference fit was applied to data in the region of the graph labeled A (where the curve rises more rapidly) and again in the region of the data were the concentration rises more slowly (labeled B). Derived diffusion coefficients are shown in Table 1. Each diffusion coefficient is the result of at least three independent experiments as indicated by the error bars.

The data are shown graphically in Fig. 5. For the PEG free experiment the diffusion coefficients measured for $Ru(NH_3)_6^{3+}$ in regions A and B fall within experimental error of each other (Fig. 5), while the diffusion coefficients for $Ru(NH_3)_6^{3+}$ in regions A and B in the presence of PEG are measurably different. In all cases, the initial penetration (dotted bars) of $Ru(NH_3)_6^{3+}$ in the presence of

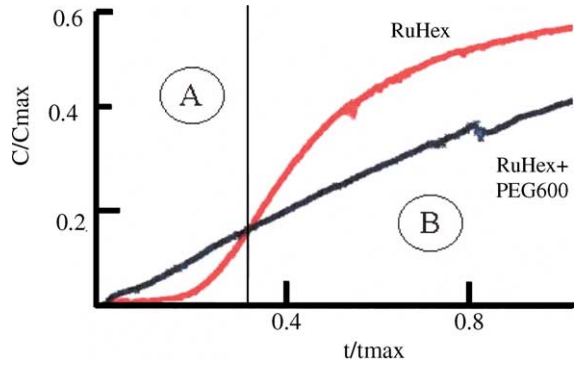

Fig. 4. The relative concentration of $Ru(NH_3)_6^{3+}$ in the acceptor cell is plotted as a function of relative time. The donor cell $Ru(NH_3)_6^{3+}$ concentration is 5 mM. The donor cell also contains 5% PEG 600. Both donor and acceptor cells contain 0.1 M NaCl. Dry clay film thickness is 33 μm. The rate of transport is initially fast and then slows. A single diffusion coefficient is insufficient to model this system and diffusion coefficients were modeled in regions "A" (before cross over) and "B" (after cross over).

PEG exceeds that of $Ru(NH_3)_6^{3+}$ in the absence of PEG. With time the rate of penetration decreases for PEG up to PEG 1500 suggesting that the film is becoming more impenetrable or blocked. PEG of 4600 and 10 K show decreased penetration compared to the initial value although penetration exceeded that of the PEG free experiments.

The dramatic change in behavior with increasing chain length can be attributed to size exclusion effects. The oligomer lengths along the *c*-axis were calculated (Table 1) using the following equation:

$$\lambda = \frac{1}{44} M \lambda_0 \quad (3)$$

where $\lambda_0 = c/7 = 2.783$ Å is the length of one monomer unit in the crystal unit cell (unit cell parameters compiled from X-ray diffraction data of Nettesheim (Nettesheim et al. [18]) and M is the average molecular weight. These oligomer lengths should be compared to the interlayer distance for SWy-1 in 0.1 M NaCl bathing electrolyte, 20–60 Å. The dimensions of the PEG suggest that PEG 200, PEG 600, and possibly PEG 1500 easily access the interlayer domain of the clay while PEG 4600 and PEG 10,000 are size excluded. The rate of penetration should change dramatically between PEG 600 and PEG 4600 with PEG 4600 and PEG 10,000 needing to "reptate" to intercalate into the clay. This data is consistent with studies by Parfitt (Parfitt and Greenland [19]) which showed that the greater the molecular weight of the PEG the longer it takes to be adsorbed by the clay. They determined that after 2 h absorption of PEG 600 into Wyoming montmorillonite was complete but a week was required for the same amount of PEG 20,000 to be adsorbed. Aranda (Aranda and Ruiz-Hitxky [20]) found that PEOs and PEGs of MW 600–600,000 intercalated with rates inversely proportional to the MW. After three days equilibration PEG 600 had adsorbed 513 meq of oxyethylene units (OEUs)/100 g of sodium exchanged clay while PEG 10,000 had adsorbed 160 OEUs/100 g. Intercalation has been identified as occurring between the exchangeable ions on the clay surface and the non-terminal portion of the glycol (Reid and Dolan [4]). Other related studies indicate that PEG 1500 can be adsorbed to silica to form dendritic monolayers. Upon thermal annealing the dendritic monolayers collapse to three-dimensional micro-droplets upon the surface (Nettesheim, Zeisel [18]).

These data suggest that there should be a transition in the structure of the PEG within the clay observed between PEG 600 and PEG 4000 as embodied in PEG 1500. Structure of PEG in clay can be monitored by IR. Attempts made to perform transmission IR on films post experiment failed due to the fragility of the films. Thicker films were formed on the meshes and transmission IR data obtained. In Fig. 6, films formed from clay impregnated with variable amounts of PEG 600 (fully intercalatable) and PEG 1500 (marginally intercalatable) are compared. Bands at 3621 cm^{-1} associated with AlOH, 3346 cm^{-1} associated with OH stretching of hydrated water (Van den Marel and Beutelspachen [21]; Van Olphen and Fripiat [22]) were monitored for the exchange of PEG with water. The intercalation of PEG was monitored at 2873–2900 cm^{-1} via an increased in the (CH group). When PEG is added in small weight percents the water band is diminished consistent with data shown for the intercalation of crown ether (Ruiz-Hitzy and Casal [23]). No major differences between the two PEG were observed with the reduction of water as the percent PEG increased from 0 to 15%, however it was noted that the amount of water in the PEG 600 films increased with PEG >35% more so than in films containing PEG 1500. This is consistent with the observation that desorption of interlayer water is not complete and that 25% of water remains in clay when PEO is intercalated (Manias et al. [24]).

Table 1
Measured diffusion coefficients for $Ru(NH_3)_6^{3+}$ in SWy-1 clay

Probe solution (5 mM $Ru(NH_3)_6^{3+}$, 0.1 M NaCl, 5% PEG)	λ (Å) *c*-axis	D_A (cm^2/s)	S.D.$_A$	D_B (cm^2/s)	S.D.$_B$
No PEG	0	4.6E−07	0.7E−07	5.1E−7	0.2E−07
PEG 200	13	7.0E−07	1E−07	4.7E−07	0.5E−07
PEG 600	38	6.9E−07	0.6E−07	3.7E−07	1E−07
PEG 1500	95	5.5E−07	1.1E−07	3.3E−07	2E−07
PEG 4600	291	8.9E−07	0.9E−07	6.0E−07	0.3E−07
PEG 10,000	633	7.3E−07	1.0E−07	5.7E−07	2E−07

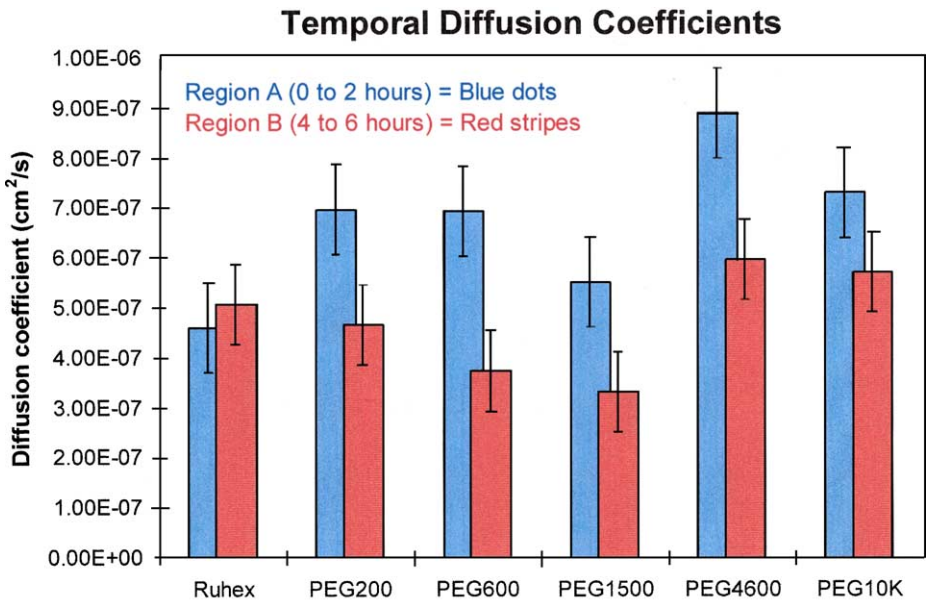

Fig. 5. A plot of the measured diffusion coefficients of $Ru(NH_3)_6^{3+}$ across a 33 μm (dry thickness) clay film in the presence of 5 mM $Ru(NH_3)_6^{3+}$, 0.1 M NaCl, and 5% PEG solutions. The solid black values represent diffusion coefficients measured within the first portion of the experiment (region A in Fig. 4B) and the hatched bars represent the diffusion coefficient modeled from the data obtained at the final portion (approximately 10 h) of the experiment (region B in Fig. 4B). The error bars represent three separate experimental runs.

The conformation of the PEG within the film can be monitored for the 1500 MW PEG by following the crystalline helical splitting at 1359 and 1344 cm^{-1} associated with the CH_2 gauche wag (Olienike and Snikolopyan [25]; Rabolt et al. [26]) and the 1324 cm^{-1} CH_2 trans wag (Bailey and Koleske [27]). Replacement of helical splitting 1359 and 1344 cm^{-1} by a single broad gauche band at 1351 cm^{-1}, a feature associated with the gauche CH_2 wag in the molten state. Interestingly, the crystal form of the polyene shows a small trans (1324 cm^{-1} attributed to the CH_2 wag) feature not observed in the intermediate weight percent spectra but which is observed again at the lowest weight percent

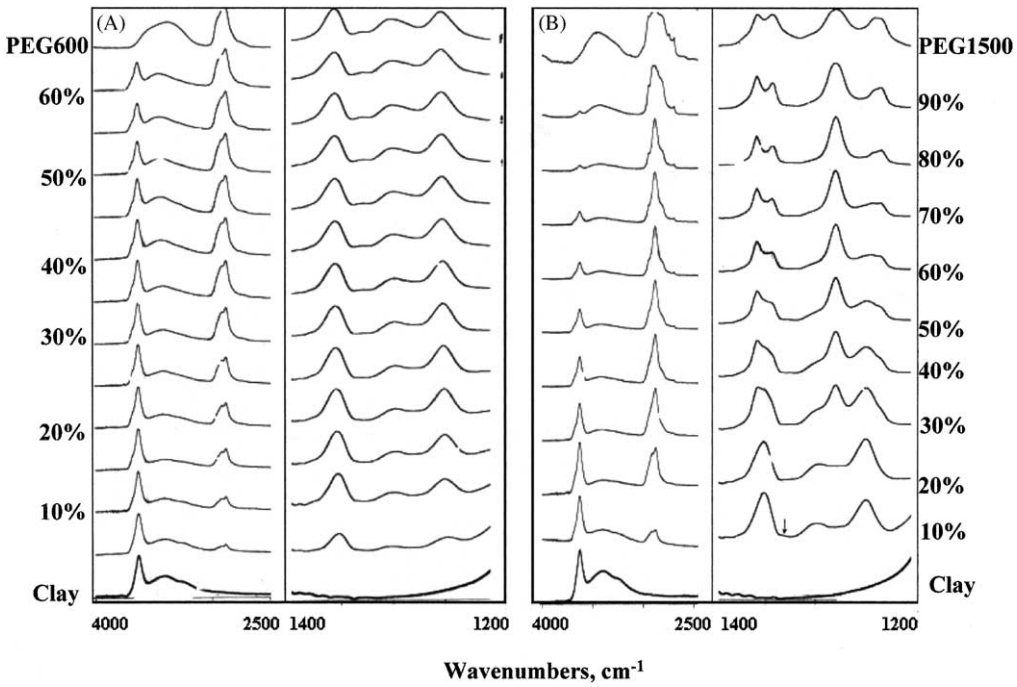

Fig. 6. IR spectra obtained from clay PEG slurries dried onto Pt mesh. The amount of PEG was varied from 0 to 60% or 100% for two different PEG species.

addition. This data is consistent with other data which has found that crystallites form in these matrices as noted by the small size of the Li-Mont PEO 100,000 MW interlayer size (8.2 Å) (Vaia et al. [24]). It was observed that 5% PEG intercalated clays showed low interlayer spacings (14–17.5 Å), a distance sufficient to prevent further water entrance into the clay.

Also of interest was the fact that PEG 600 showed no major change in conformation with increasing PEG loading in the film in contrast to the PEG 1500. This data suggests that the lower molecular weight PEG do not fully desolvate the clay and are in flux upon increasing loading (as would occur during our transient loading experiments) while the transitional PEG 1500 begins to solidify and fully block the film.

A model based on the wire mesh supported clay film diffusion absorbance and IR experiments is shown in Fig. 7. The cartoon indicates that in the absence of PEG the diffusion of the probe molecule through the film has little impact on film structure for the time monitored, and, hence, there is a little change in the measured diffusion coefficient. When the film is simultaneously exposed to low molecular weight PEG there is initial disruption of the film via intercalation of coiled chains and loss of water leading to enhanced permeation. With time the short molecular weight chains move about and link clay platelets, decrease permeation of the probe, and water can be reinserted into the film. For large molecular weight PEG, long chains attach to external surfaces disrupting the organization of the film, increasing diffusion of the probe, and decreasing water within the film. At longer times, the large molecular weight PEG can reorganize to a more crystalline form, however the bulk structure of the film remains disrupted and permeation of the probe remains high.

Because the supported film experiments are relatively long (12 h duration, not including film preparation) and because the films are relatively fragile (50% failure rate), alternative experiments were performed in which the film is supported upon a Pt electrode in a clay-modified electrode experiment (Macha and Fitch [15]). This experiment does not fully mimic a true sink/source experiment but has the advantage of greater robustness. The penetration of $Ru(NH_3)_6^{3+}$ is monitored by the reversible oxidation/reduction of the $Ru(NH_3)_6^{3+}$ probe molecule at the clay coated Pt electrode.

The cyclic voltammetric peak height for a Pt disk electrode is a measure of both the concentration of the probe within the film which is controlled by the partition coefficient, κ and the diffusion coefficient of the probe within the clay film, D_f:

$$i_p = n^{3/2} F A v^{1/2} \kappa C D_f^{1/2} = 2.69 \times 10^{-3} A v^{1/2} \kappa C D_f^{1/2} \quad (4)$$

where i_p is the peak current (A), n the number of electrons involved in the oxidation/reduction (1 for $Ru(NH_3)_6^{3+}$),

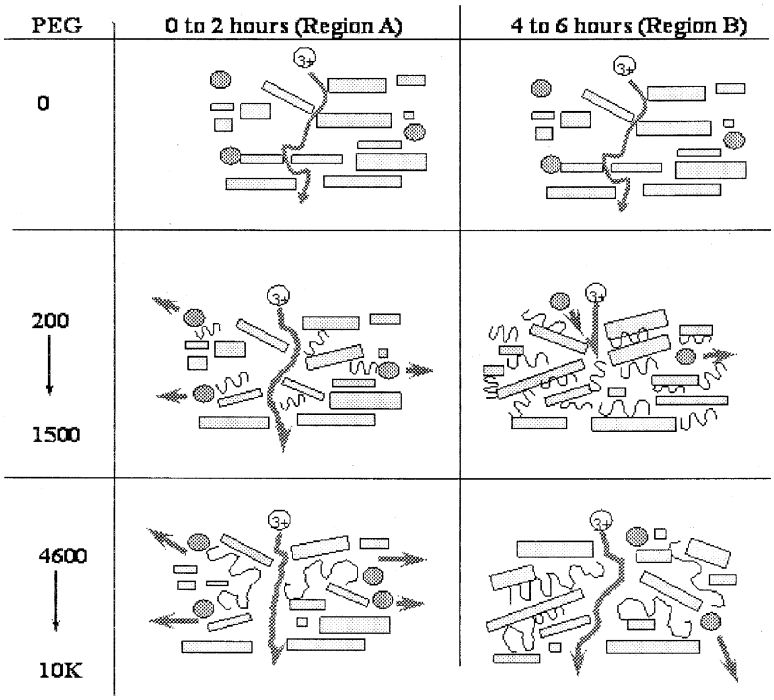

Fig. 7. Cartoon schematic of film structural changes during time for films exposed to no PEG, PEG of molecular weights 200–1500, and PEG of molecular weights 1500–10,000. No structural changes are observed in the absence of PEG. Low molecular weight PEG is intercalated into the clay, expels water, and disrupts the structure increasing permeation. With time the PEG helps bind platelets together and some water in sealed within the film. High molecular weight PEG does not readily intercalate, but does expel water from exterior surfaces and disrupt the structure. With time the PEG reorganizes into more crystalline domains but film structure remains disrupted.

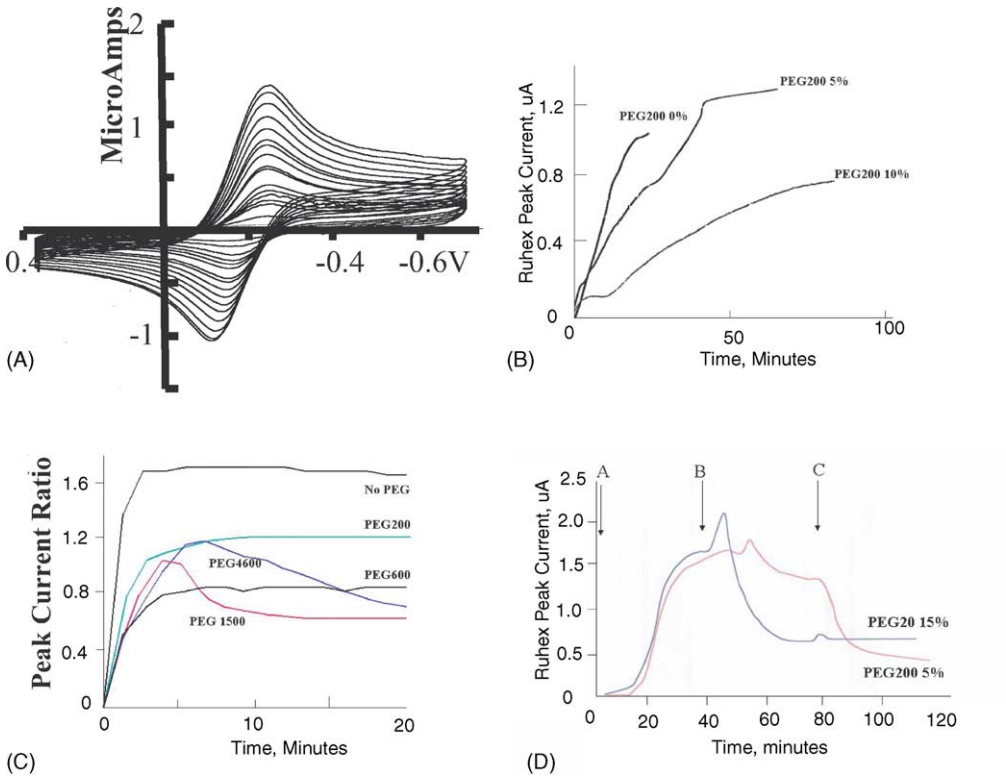

Fig. 8. (A) A series of cyclic voltammograms for the oxidation/reduction of $Ru(NH_3)_6^{3+}$ (3 mM solution in 0.1 M NaCl with 5% 200 PEG) obtained for a 35 μg clay film showing the uptake of the probe molecule. (B) Cathodic peak current for $Ru(NH_3)_6^{3+}$ (3 mM solution in 0.1 M NaCl) obtained as a function of time as a dry clay film (35 μg) is exposed to $Ru(NH_3)_6^{3+}$ solution in the presence and absence of PEG. The decreased amount of time required to observe the transport of $Ru(NH_3)_6^{3+}$ as compared to the optical experiments is consistent with the smaller film thickness used in the clay-modified electrode experiments. (C) A plot of peak current ratio (peak current at the clay-modified electrode divided by the peak current at the bare electrode) for $Ru(NH_3)_6^{3+}$ as a 17.5 μg clay- modified electrode is exposed to solutions of 3 mM $Ru(NH_3)_6^{3+}$, 0.1 M NaCl, and 5% PEG of variable molecular weight. (D) Peak cathodic current for $Ru(NH_3)_6^{3+}$ as a function of time as a 35 μg dry clay-modified electrode is first exposed to 3 mM $Ru(NH_3)_6^{3+}$ in 0.1 M NaCl (time A) and then to a solution of 15% PEG 200 or 5% PEG 200 (time B). The solution is finally exposed to a 0.1 M NaCl wash solution (time C).

F the Faraday's constant (9.6484×10^4), A the area of the electrode (cm^2), v the scan rate (V/s), κ the partition coefficient, C the concentration of the compound in solution (mol/cm^3), and D_f is the diffusion coefficient in the film (cm^2/s). For most clay-modified electrode experiments, the variables $\kappa CD_f^{1/2}$ can not be independently determined.

The cathodic peak height for $Ru(NH_3)_6^{3+}$ as it moves into a 35 μg film in the presence of 0.1 M NaCl (Fig. 8A) is plotted as a function of time in Fig. 8B in the presence of PEG 200 at three different solution PEG concentrations. The time frame for this experiment is approximately 1 h compared to the 10–12 h for the absorbance experiments consistent with the 1/3 film thickness. Using the diffusion coefficient for $Ru(NH_3)_6^{3+}$, as determined by the absorbance cell experiments, the area of the electrode (7.85×10^{-3} cm^2), the scan rate of the experiment (0.05 V/s), and the steady state current for $Ru(NH_3)_6^{3+}$ (1.7 μA), the parameter κC for $Ru(NH_3)_6^{3+}$ within the film can be calculated to be 5.84×10^{-3} M. The expected concentration within the film in response to the CEC and the estimated wet film distance (expansion of a factor of 40 (Kelly [3]) is 3.7×10^{-3} M resulting in a partition coefficient, κ, of <2. The order of magnitude of κ is consistent with other estimates.

In Fig. 8B, we see that the addition of PEG from 0 to 10% in the bulk solution causes the $Ru(NH_3)_6^{3+}$ signal to develop more slowly. The decrease in current indicates that $\kappa CD_f^{1/2}$ for $Ru(NH_3)_6^{3+}$ has decreased in the presence of PEG. $\kappa CD_f^{1/2}$ decreases due to decreases in partitioning of $Ru(NH_3)_6^{3+}$ into the clay film and/or a decrease in its diffusion once inside the film. Both the processes are probable. The slower development of the signal provides corroborating evidence for the decreased D_f with time observed in the absorbance experiments.

The effect of solutions of the probe molecules also containing 5% of different PEG molecular weight is shown in Fig. 8C using a thinner film (17 μg). The time frame of these experiments is, therefore, shorter, but the relative trends are similar. Note that $\kappa CD_f^{1/2}$ for $Ru(NH_3)_6^{3+}$ changes in the presence of PEG. Penetration of $Ru(NH_3)_6^{3+}$ into the film is initially rapid in all cases. In Fig. 8C, the currents are normalized to the bare electrode. The normalized current maxima depend on the PEG molecular weight and are a function

of the increased concentration of the probe molecule within the clay film, as compared to a steady state equilibration across the film. As a consequence, absolute signal height is not a reliable diagnostic. However, the electrochemical experiment replicates the data obtained by the absorbance cell experiment in that the system changes character under the onslaught of the PEG, particularly noted for PEG 1500 and PEG 4600.

The decay in the $Ru(NH_3)_6^{3+}$ normalized signal in Fig. 8C with time for the PEG 1500 and PEG 4600 can be interpreted as either a decrease in the film concentration (replacement by the PEG) or by sealing of the $Ru(NH_3)_6^{3+}$ into the film with subsequent decrease in diffusion coefficient. We believe that the $Ru(NH_3)_6^{3+}$ is expelled because of the continuously falling signal observed. Deliberate sealing of the film was observed only when the film was first exposed to the $Ru(NH_3)_6^{3+}$ and then subsequently exposed to a large concentration of the PEG (15%). At 15 wt.% solution, the PEG formed a dense layer in the bottom of the cell and immersion of the tip of the electrode into the film appeared to "seal" the $Ru(NH_3)_6^{3+}$ in the film, as observed by steady state signals even in the presence of a flush of fresh electrolyte (Fig. 8D). In Fig. 8D, a film of 35 μg clay was used.

These data indicate that both methods (supported thin film diffusion experiments via absorbance and clay-modified electrodes experiments) are reliable predictors of the effect of PEG on penetration of electrolyte into thin clay films. The absorbance cell experiments have the advantage of being extendable to a wider range of probe molecules and to a full mathematical analysis of the diffusion coefficients. The clay-modified electrode experiments have the advantage of speed and robustness and the disadvantage in that the signal depends upon $\kappa C D_f^{1/2}$ as opposed to D_f as an independent variable. Both experiments indicate that there is a dramatic difference in behavior when the PEG MW extends to 1500 and above suggesting that the penetration of $Ru(NH_3)_6^{3+}$ is initially more rapid than the penetration of the PEG. "Sealing" of the film can be effected by PEG 1500 or by a flush of high concentration of the lower molecular weight PEG. As the concentration of PEG 1500 within the film increases, the structure moves from a liquid state to a solid state and water content remains low.

The comparison of the absorbance cell data with the electrochemical data leads to the conclusion that the signals obtained by the electrochemical experiment are a convolution of the film diffusion coefficient and the concentration of the probe molecule within the film.

References

[1] C. Durand, T. Forsans, C. Ruffet, A. Onaisi, A. Audibert, Rev. L. Inst. Fr. Petrole 50 (2) (1995) 187–218.
[2] L. Bailey, M. Keall, A. Auibert, J. Lecourtier, Langmuir 10 (5) (1994) 1544–1549.
[3] J. Kelly, Oil Gas J. (1968) 67–70.
[4] P.I. Reid, B. Dolan, Presented at the SPE International Symposium on Oilfield Chemistry, 1995, p. 155.
[5] J. Qui, A. Fitch, J.S. Baker, R. Lucas, in: H. Kodama, A.R. Mermutand, J.K. Torrance (Eds.), Proceedings of the 11th International Clay Conference: Clays for our Future. ICC97, Ottawa, 1999, pp. 351–355.
[6] A. Fitch, J. Du, J. Electroanal. Chem. 319 (1991) 409.
[7] A. Fitch, P. Subramanian, J. Electroanal. Chem. 362 (1993) 177.
[8] E. Azaz, R. Segal, J. Pharm. Pharmacol. 29 (1976) 322–323.
[9] H.W. Chang, E. Bock, Anal. Biochem. 104 (1980) 112–117.
[10] R.H. Grim, Clay Mineralogy, McGraw-Hill, New York, 1968.
[11] A. Fitch, A. Lavy-Feder, S.A. Lee, M.T. Kirsh, J. Phys. Chem. 92 (23) (1988) 6665–6670.
[12] P. Joo, A. Fitch, Environ. Sci. Technol. 30 (9) (1996) 2681.
[13] P. Subramanian, A. Fitch, J. Electroanal. Chem. 26 (1992) 1775.
[14] A. Macha, G. Zayia, J. Du, J. Stein, A. Fitch, Appl. Clay Sci. 15 (1999) 153–172.
[15] S.M. Macha, A. Fitch, Mikrochim. Acta 128 (1998) 1–18.
[16] A. Fitch, Y. Wang, S.-H. Park, M. Marjanski, in: J. Leddy, R.M. Wightman (Eds.), New Directions in Electroanalytical Chemistry, The Electrochemical Society, Pennington, NY, 1996, pp. 248–262.
[17] J. Qiu, G. Villemure, J. Electroanal. Chem. 395 (1) (1995) 159.
[18] S. Nettesheim, D. Zeisel, M. Landschuh, R. Zenobi, Langmuir 14 (11) (1998) 3106.
[19] R.L. Parfitt, D.J. Greenland, Clay Miner. 8 (1970) 305–315.
[20] P. Aranda, E. Ruiz-Hitzky, Chem. Mater. 4 (1992) 1395–1403.
[21] H.R. Van den Marel, H. Beutelspachen, Elsevier Press, New York, 1976.
[22] H. Van Olphen, J.J. Fripiat, Data Handbook for Clay Materials and other Nonmetallic Minerals, Pergamon Press, NY, 1979.
[23] E. Ruiz-Hitzy, B. Casal, Clay Miner. 21 (1986) 1–7.
[24] E. Manias, Z. Panagiotopoulos, D.B. Zax, E.P. Giannelis, in: A. Fitch (Ed.), Electrochemical Properties of Clays, vol. 10, The Clay Minerals Society, Aurora, CO, 2002, pp 185–205.
[25] E.F. Olienike, N.S. Snikolopyan, J. Polym. Sci. C 15 (1968) 3677.
[26] J.F. Rabolt, K.W. Johnson, R.N. Zitter, J. Chem. Phys. 61 (2) (1974) 504.
[27] L. Bailey, J.F. Koleske, Poly(ethylene oxide), Academic Press, New York, 1976.